Inorganica Chimica Acta 374 (2011) 197–204

Contents lists available at ScienceDirect

Inorganica Chimica Acta

journal homepage: www.elsevier.com/locate/ica

Non-covalent interactions between cations in the crystal structure of [Pt{4′-(*p*-tolyl)trpy}Cl]SbF_6, where trpy is 2,2′:6′,2″-terpyridine, underpin the salt's complex solid-state luminescence spectrum

John S. Field, Colin R. Wilson, Orde Q. Munro *

School of Chemistry, University of KwaZulu-Natal, Private Bag X01, Pietermaritzburg 3201, South Africa

ARTICLE INFO

Article history:
Available online 22 March 2011

Dedicated to our good friend and colleague, Wolfgang Kaim, in recognition of his considerable contributions to Coordination Chemistry.

Keywords:
Platinum(II) complexes
Terpyridine
X-ray structure
Luminescence
π-Stack
MMLCT

ABSTRACT

The synthesis and characterization of [Pt{4′-(*p*-tolyl)trpy}Cl]SbF_6 is described where trpy is 2,2′:6′,2″-terpyridine. A single crystal X-ray structure determination at 100 K shows that the cations are stacked in columns that comprise cations arranged in a staircase motif. Successive cations within a column are linked by π(trpy)–π(phenyl) stabilizing interactions; and each cation in one column is linked to a cation in an adjacent column by a weakly stabilizing Pt···Pt interaction. The Pt···Pt distance is 3.434(1) Å. The metrics governing non-covalent interactions between [Pt{4′-(aryl)trpy}Cl]$^+$ cations have been analyzed for the present structure and related structures in the CSD (Cambridge Structural Database). Cation dimers cluster into three distinct groups based on their lateral shifts and, to a lesser extent, the angular parameters governing their relative displacements; the dominant grouping exhibits Pt···Pt and π(trpy)–π(trpy) stabilizing interactions. An emission spectrum recorded at 77 K on a solid sample of the compound is best interpreted as arising from the decay of three photoexcited states: a ^{3}MLCT (MLCT = metal-to-ligand charge transfer) state; a ^{3}MMLCT (MMLCT = metal–metal-to-ligand charge transfer) state, and an excimeric $^3\pi$–π^* state.

1. Introduction

The [Pt{4′-(*p*-tolyl)trpy}Cl]$^+$ cation (trpy = 2,2′:6′,2″-terpyridine) was first reported as the perchlorate salt by Yip and co-workers in 1993 [1]. The complex exhibits moderately strong ^{3}MLCT (MLCT = metal-to-ligand charge transfer) emission in degassed acetonitrile ($10^3\varphi$ = 0.7, λ_{em}(max) = 561 nm, τ = 2.4 μs) [1]. These properties make the complex useful as a photocatalyst for the production of hydrogen from Hantzsch 1,4-dihydropyridines [2] and water [3]. Of interest here however, are the photophysical properties of the complex in the *solid state*, in particular of the hexafluoroantimonate(V) salt, [Pt{4′-(*p*-tolyl)trpy}Cl]SbF_6 (Scheme 1). Our interest in the hexafluoroantimonate(V) salt was stimulated by an X-ray diffraction study, which showed that the cations stack in an unusual "double staircase" motif, with both intermolecular π–π and Pt···Pt stabilizing interactions present in the crystal. Previous work has shown that intermolecular interactions of this type can play an important role in determining the photophysical properties of ionic terpyridyl ligand complexes of platinum(II) in the solid state [1,4–13]. However, the precise role is crystal structure dependent, and we wished to elucidate the relationship between the novel crystal structure for the title compound and its emission properties in the solid state.

2. Experimental

The 4′-(*p*-tolyl)trpy ligand was synthesised following the general method described by Kröhnke [14] and given in detail in Ref. [5] for closely-related ligands. The [Pt(PhCN)$_2$Cl$_2$] starting complex and the $AgSbF_6$ salt were obtained from Strem Chemicals Inc. and used without further purification. The acetonitrile for the complex synthesis and crystal growth was of the Chromosolv™ HPLC grade from Aldrich and used as received. The diethyl ether was from Saarchem and of the uniLAB™ grade and also used as received.

2.1. Synthesis and characterization of [Pt{4′-(*p*-tolyl)trpy}Cl]SbF_6

A suspension of $AgSbF_6$ (0.138 g, 0.40 mmol) and [Pt(PhCN)$_2$Cl$_2$] (0.217 g, 0.46 mmol, 15% molar excess) in acetonitrile (30 mL) was refluxed under dry nitrogen for 24 h and then cooled to room temperature. The AgCl precipitate was separated by cannula transfer of the solution though a frit, and a concomitant transfer of the filtrate

* Corresponding author. Tel.: +27 33 260 5270; fax: +27 33 260 5009.
E-mail addresses: fieldj@ukzn.ac.za (J.S. Field), munroo@ukzn.ac.za (O.Q. Munro).

0020-1693/$ - see front matter © 2011 Elsevier B.V. All rights reserved.
doi:10.1016/j.ica.2011.03.043

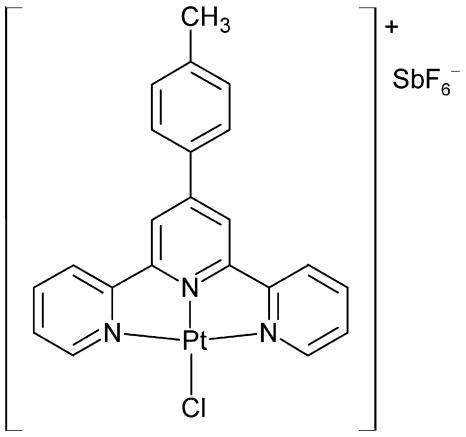

Scheme 1. Structure of the luminescent salt [Pt{4′-(*p*-tolyl)trpy}Cl]SbF_6.

to a dry flask containing a 5% excess of 4′-(*p*-tolyl)trpy (0.155 g, 0.48 mmol). This mixture was refluxed for a further 24 h. After cooling, diethyl ether was added dropwise causing precipitation of the crude product as a yellow solid that was dried *in vacuo*. Re-crystallization was by means of slow vapor diffusion of diethyl ether into a concentrated solution of the product in acetonitrile. Yield: 0.201 mg (63%). *Anal.* Calc. for $C_{22}H_{17}ClF_6N_3PtSb$ (FW = 789.68 g mol^{-1}): C, 33.46; H, 2.17; N, 5.32. Found: C, 33.53; H, 2.13; N, 5.28%. IR (KBr, cm^{-1}): ν[4′-(*p*-tolyl)trpy] 2917w, 1603s, 1551m, 1476s, 1400m, 1246s; $\nu[SbF_6^-]$ 649vs. ^1H NMR (DMSO-d_6): δ 8.74 (2H, s, $H^{3',5'}$), 8.67 (2H, d, $H^{3,3''}$), 8.59 (2H, d, $H^{6,6''}$), 8.38 (2H, t, $H^{4,4''}$), 8.00 (2H, d, $H^{2''',6'''}$), 7.77 (2H, t, $H^{5,5''}$), 7.43 (2H, d, $H^{3''',5'''}$), 2.44 (3H, s, CH_3). UV–Vis (CH_2Cl_2) λ_{max}/nm: 284, 337 (π–π^*), 397, 417 (MLCT). Emission (CH_2Cl_2, λ_{ex} = 390 nm) λ_{max}/nm: 545 (0–0), 580 (0–1).

2.2. Physical measurements

Elemental analyses were performed in the Elemental Microanalysis unit of the Department of Chemistry at the University of Durham, UK. FTIR spectra were measured using a Perkin Elmer Spectrum One spectrometer, and the samples prepared as KBr pellets. The ^1H (500 MHz) spectra were recorded on a Bruker Avance III spectrometer with chemical shifts referenced to solvent protons. The instrument used for the measurement of emission spectra was a Photon Technologies Int. (PTI) fluorescence spectrometer controlled by PTI's Felix32© Version 1.1 software [15]. The solid samples used for the emission measurements were finely ground and transferred to an NMR tube that served as the sample holder; for the purposes of the 77 K measurements the NMR tube was inserted in a PTI-supplied quartz cold finger filled with liquid nitrogen. Steady state emission spectra were recorded using PTI's XenoFlash™ 300 Hz pulsed light source and gated emission scans with a delay of 95 μs, an integration window time of 100 μs and 50 pulses per channel (shots). Detection was by means of PTI's Model 814 Analog/Photon-Counting Photomultiplier Detector. The excitation wavelength was 420 nm with the scattered light being removed by means of a suitable wavelength band-pass filter. Note that because the emission intensity was so weak (even at 77 K) it was necessary to correct the measured spectrum for background due to the glass of the NMR tube. For the lifetime measurements, the excitation source was again the Xenon flash lamp with the emission decay captured by the Photomultiplier Detector at a wavelength corresponding to the peak of interest, and analyzed by the FeliX32™ software [15].

Table 1
Crystal data, data collection and refinement details for [Pt{4′-(*p*-tolyl)trpy}Cl]SbF_6.

Empirical formula	$C_{22}H_{17}ClF_6N_3PtSb$
M_r (g mol^{-1})	789.68
Crystal size (mm)	0.05 × 0.20 × 0.40
T (K)	100
λ (Å)	0.71073
Crystal system	monoclinic
Space group	$P2_1/c$
a (Å)	7.6320(5)
b (Å)	21.907(2)
c (Å)	13.081(1)
β (°)	94.935(5)
V (Å^3)	2179.0(3)
Z	4
D_{calc} (g cm^{-3})	2.407
μ (mm^{-1})	7.844
F(0 0 0)	1480
θ Range (°)	2–32
Reflections collected (independent)	19 831 (7009)
Observed reflections [$I > 2\sigma(I)$]	6401
R_{int}	0.0478
Numbers refined parameters (restraints)	308 (0)
Final R_1 [$I > 2\sigma(I)$]	0.0504
Final wR_2 (all data)	0.1532
Maximum, Minimum $\Delta\rho$ (e Å^{-3})	3.6 (Pt), −5.3 (Pt)

2.3. Crystal structure determination and refinement

X-ray intensity data were collected with an Oxford Diffraction Xcalibur 2 CCD 4-circle diffractometer linked to an Oxford Cryostat System. The data were collected at 100 K using Mo Kα radiation (2.0 kW, 0.71073 Å), 0.75° frame widths, 20 s exposures at a crystal-to-detector distance of 50 mm, and omega 2-theta scans of −54.00–60.60° or −54.00–60.75° at θ = 30°. The data were reduced with the program CRYSALIS RED [16] (Version 170) using outlier rejection, scan speed scaling, as well as standard Lorentz and polarization correction factors. The structures were solved with SHELX-97 [17] using Patterson methods with all non-hydrogen atoms refined anisotropically with SHELX-97 [17] (using WINGX [18] as an interface). Hydrogen atoms were geometrically constrained (C–H = 1.05 Å) using the appropriate AFIX command and refined isotropically with U_{iso} fixed at 1.20 times the equivalent isotropic temperature factor for a parent sp^2 carbon atom, and 1.5 times for a parent sp^3 carbon atom. Plots were obtained with ORTEP3 for Windows [19] and MERCURY 2.3 [20]. Lattice constants, refinement details and final discrepancy indices are given in Table 1.

3. Results and discussion

The synthesis of the perchlorate salt of the [Pt{4′-(*p*-tolyl)trpy}Cl]$^+$ cation has been reported [1]. Here we report the synthesis of the hexafluoroantimonate(V) salt using methods developed in our laboratories—details of the synthesis and characterization are given in Section 2.

3.1. Crystal structure of [Pt{4′-(*p*-tolyl)trpy}Cl]SbF_6

Single crystals were grown by slow vapor diffusion of diethyl ether into a concentrated solution of the complex in acetontrile. Fig. 1 gives a perspective view of the cation with selected interatomic distances and angles included in the caption. The coordination geometry at the platinum atom is irregular square-planar, as evidenced by N1–Pt–N2 and N2–Pt–N3 angles of 81.1(2)° and 81.2(3)°, respectively; as well as by a '*trans*' N1–Pt–N3 angle of 162.3(2)°. This is typical of terpyridyl ligand complexes of platinum(II) and arises from geometric constraints imposed by the rigid tridentate ligand [1,4–13,21–23]. Also typical is that the platinum

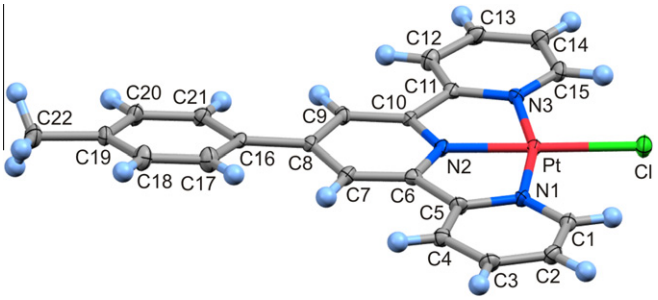

Fig. 1. MERCURY 2.3 [20] view of the cation in [Pt{4′-(*p*-tolyl)trpy}Cl]SbF_6 drawn with 50% thermal ellipsoid probabilities. Hydrogen atoms are drawn as spheres of arbitrary radius. Selected bond lengths (Å) and angles (°) are: Pt–N1, 2.007(5); Pt–N2, 1.931(5); Pt—N3, 2.027(5); Pt—Cl, 2.297(2); N1—Pt—N2, 81.1(2); N1–Pt–N3, 162.3(2); N1–Pt–Cl, 98.3(2); N2–Pt–N3, 81.2(2); N2–Pt–Cl, 178.7(2); N3–Pt–Cl, 99.4(2).

to bridgehead nitrogen distance of 1.931(5) Å is shorter than the distances from the Pt atom to the outer nitrogen atoms of 2.007(5) and 2.027(5) Å [1,4–13,21–23]. The Pt–Cl distance of 2.297(2) Å fits with Pt–Cl distances reported for other terpyridyl ligand complexes of platinum where the co-ligand is a chloride ion [1,4–6,9,10]. Of particular interest is that the *p*-tolyl group twists slightly out of the plane of the trpy moiety, as evidenced by a dihedral angle of only 9.3° between mean planes through the non-H atoms of the trpy moiety on one hand, and those of the phenyl ring on the other. The cation as a whole is consequently approximately planar, with a maximum deviation for any one non-H atom from a mean plane drawn through all the non-H atoms comprising the cation of 0.16 Å (Cl). In fact, it is because the trpy moiety has been extended by the addition of a co-planar *p*-tolyl group that intermolecular π(trpy)–π(phenyl) interactions are made possible; without these stabilizing interactions, the novel crystal structure could not exist.

The overall packing of the [Pt{4′-(*p*-tolyl)trpy}Cl]$^+$ cations and SbF_6^- anions is illustrated in Fig. 2, which shows a projection of the unit cell contents down the *a*-axis of the unit cell. With this view it is easily seen that the cations and anions occupy separate columns parallel to the *a*-axis of the unit cell. Note that the columns of cations stack, one after the other, along lines parallel to the vertical axis of the diagram, i.e. there are rows of cation columns perpendicular to the unit cell *b*-axis. Furthermore, successive rows of cation columns are separated by SbF_6^- anions along the *b*-axis. From this description of the crystal packing it becomes clear that in order to understand potential cation–cation interactions, we need to investigate close contacts between cations within a column, as well as close contacts between cations from neighboring columns along a row. To this end, Fig. 3 depicts a side-view of four cation columns belonging to one row of columns. With this view it becomes apparent that successive cations within a column are laterally offset from each other, such that they take on the appearance of steps in a staircase. Close inspection of Fig. 3 also suggests that there is a close contact between a Pt atom in the first staircase and a Pt atom in the second staircase, i.e. a step in the first staircase is linked to a (lower) step in the second staircase (Fig. S1, Supporting Information, offers an enhanced view of these interactions). The third and fourth staircases are similarly linked. (We examine the Pt···Pt interaction in detail below: see Fig. 4b). Note that there is no evidence for short contacts between the second and third staircases, specifically no contacts that allow for π–π or Pt···Pt interactions. Thus, a more descriptive term for the cation packing would be that they stack in rows of inversion paired "double staircases" perpendicular to the *b*-axis of the unit cell.

We now examine the precise nature of the intermolecular interactions within a staircase and between staircases. To this end, views perpendicular to the cation 25-atom mean planes (calculated using all aryl ring atoms and the Pt(II) ion of a cation to define its mean plane) are shown in Fig. 4: in part (a) for two adjacent cations (steps) in one staircase and in part (b) for cations from adjacent staircases that are linked by the short Pt···Pt contact. In Fig. 4a the two cations are laterally offset such that π(trpy)–π(phenyl) overlap occurs at the edges of an outer pyridine ring of one cation and the phenyl group of the other cation; the non-interacting Pt atoms are separated by 7.6320(6) Å, giving an indication of the magnitude of the lateral offset. As noted by Hunter and Saunders [24] and by Janiak [25], this has as a result that π–σ attractive forces dominate between the two aromatic rings: thus, this is a stabilizing interaction. Consistent with this is that the perpendicular distance (interplanar spacing) between the cation 25-atom mean planes is 3.394(1) Å, a value that is well below the upper distance limit of 3.8 Å for a stabilizing π–π interaction between adjacent aromatic species [24,25]. Important to note is that this interaction

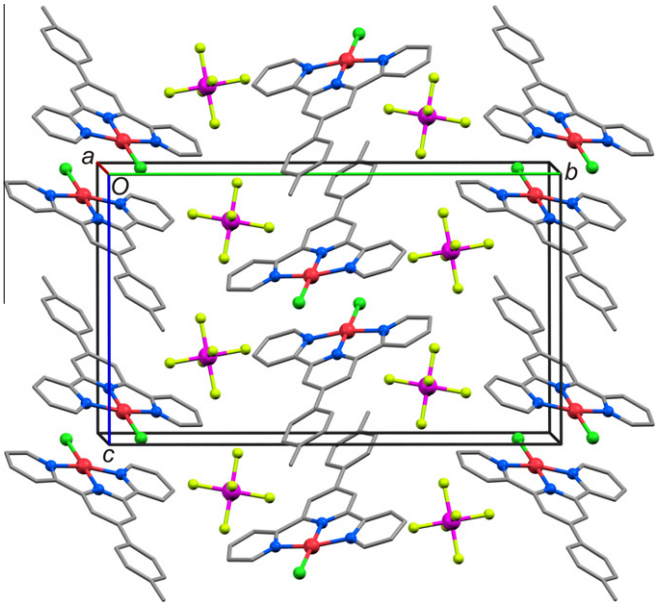

Fig. 2. View of the packing of cations and anions in [Pt{4′-(*p*-tolyl)trpy}Cl]SbF_6 drawn as a projection approximately down the *a*-axis of the unit cell. Hydrogen atoms have been omitted for clarity; non-C atoms are rendered as spheres; C atoms are located at bond intersections and have been rendered as cylinders along with all other bonds.

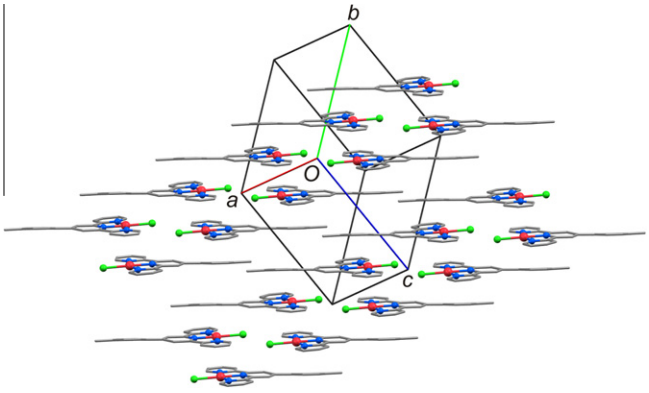

Fig. 3. Side-view of two adjacent cation "double staircases": see Section 3.1. Note that successive cations within a "staircase" are linked by a unit cell translation along the *a*-axis. Hydrogen atoms have been omitted for clarity; non-C atoms are rendered as spheres; C atoms are located at bond intersections and have been rendered as cylinders along with all other bonds.

would not be possible unless the *p*-tolyl group were present *and* approximately co-planar with the trpy moiety: it is the key interaction on which the staircase motif is built. In Fig. 4b we see that the Pt atoms of the two linked cations (an inversion pair) are nearly eclipsed. This fact, as well as the Pt···Pt distance of 3.434(1) Å, suggest that there is a stabilizing interaction between the two Pt atoms [5,9,10,26,27]. However, the interaction is likely a weak one because the Pt···Pt distance is near the upper distance limit of ~3.5 Å usually taken to indicate a finite $d_z^2(Pt)$—$d_z^2(Pt)$ orbital interaction [28]. Also apparent from Fig. 4b is that there is π(trpy)–π(trpy) overlap at the leading edges of the outer pyridine rings of the two cations. This overlap geometry also supports a stabilizing π–π interaction, as does the interplanar spacing (25-atom mean planes) of 3.268(1) Å [24,25]. A more detailed diagram of these interactions, both within the π-stacked dimer of Fig. 4b and within the linear chain to which the dimer belongs in the crystal lattice, is shown in Supporting Information (Fig. S2). Each dimer is clearly related to the next dimer in the array by an inversion operation as well as inequivalent translations (a large lateral shift and shorter perpendicular shift) in two orthogonal directions in the lattice. These symmetry operations result in a linear chain of discrete dimers related by a significant lateral shift (13.79 Å) and an interdimer (or dimer···dimer) perpendicular displacement of 3.753(1) Å (based upon the separation between the 19-atom Pt(trpy) mean planes). In short, straightforward lateral shifts applied to a perfect linear-chain structure with a single infinitely repeating Pt···Pt interaction distance, e.g., as found in $[PtCl_2(bpy)]$ [28a], where bpy = 2,2′-bipyridine, would be insufficient to generate the rather more complex array of dimers observed for the $[Pt\{4'\text{-}(p\text{-tolyl})trpy\}Cl]^+$ cations in this system. Finally, it is not unreasonable to suggest that although the stabilizing π–π and Pt···Pt intermolecular interactions seen here are energetically weak compared to the ionic interactions in the crystal lattice, they play a crucial role in aligning and discretely spacing the chromophores in the solid-state; these more subtle interactions will, in fact, be the primary determinants of the emission properties of the polycrystalline material (*vide infra*).

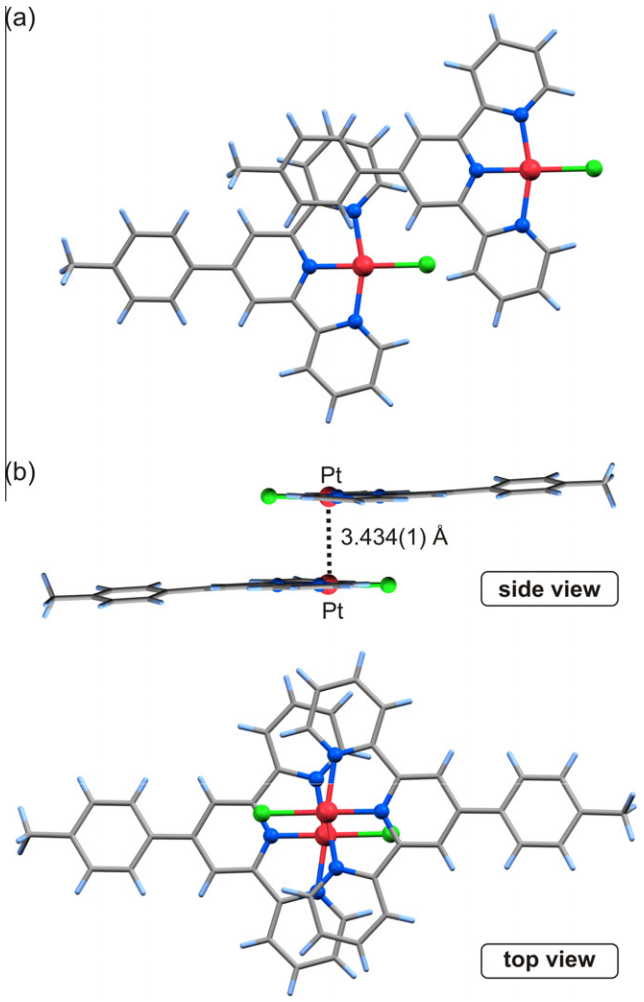

Fig. 4. Views of nearest neighbor cations: (a) within a staircase and (b) from two different staircases; see Section 3.1. Top and side views are perpendicular and parallel to the cation mean planes, respectively. Carbon and hydrogen atoms have been rendered as cylinders at bond intersects and termini, respectively. All other atoms are rendered as spheres.

3.2. Analysis of the structures of $[Pt\{4'\text{-}(aryl)trpy\}Cl]^+$ cation pairs/stacks in the Cambridge Structural Database (CSD)

To examine the precise metrical parameters between symmetry-related $[Pt\{4'\text{-}(aryl)trpy\}Cl]^+$ cations when paired in dimers or stacks more generally than those discussed above for $[Pt\{4'\text{-}(p\text{-}$

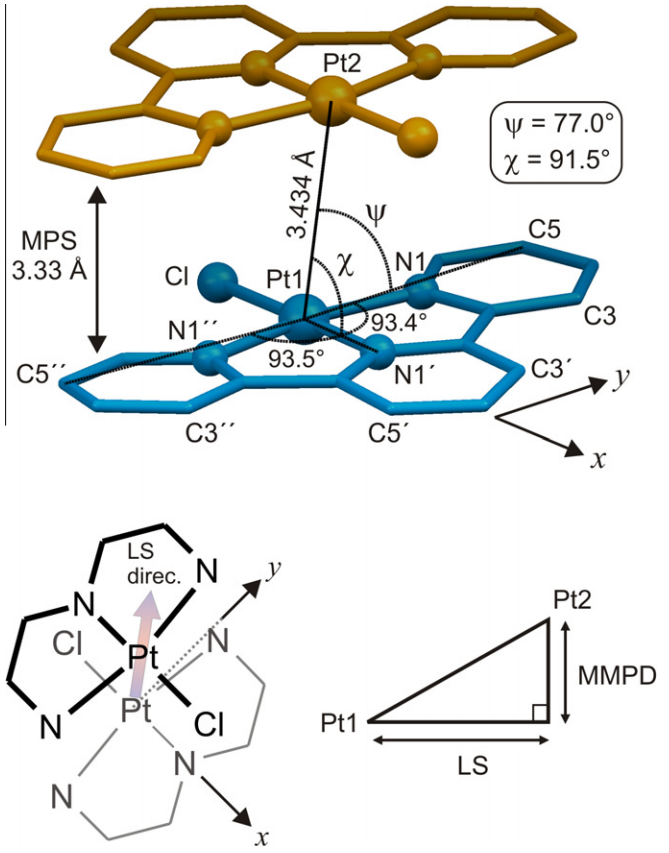

Fig. 5. Top: interaction between two $[Pt(trpy)Cl]^+$ cations (taken and simplified from the inversion pair illustrated in Fig. 4b). Metrical parameters that define the interaction geometry are indicated. The mean plane separation (MPS) is the perpendicular distance between the two 19-atom mean planes of the cations (excluding the chloride ions). The *x*-direction is defined as lying along the Pt1—N1′ bond vector. The *y*-axis direction is slightly off (3°) the direction defined by the Pt1—C5 vector (being located between this vector and the Pt1—N1 bond vector). The Pt2···Pt1···C5 angle is within 0.2° of the Pt2···Pt1—(*y*-axis) angle and may be used as a convenient approximation of this angle. Bottom left: Illustration of the lateral shift (LS) direction when a dimer is viewed perpendicular to the *xy* plane. The top Pt(II) chelate is drawn with thick bonds; the top Pt(II) ion may be located anywhere on the circumference of a circle in a plane above the lower Pt(II) ion. Bottom right: relationship between the LS, metal-to-metal perpendicular displacement (MMPD), and Pt1···Pt2 vector. Triangulation from the Pt1···Pt2 vector gives the *x*- and *y*-components of the LS vector; its scalar magnitude is calculated from the Pythagorean relationship $LS = \{LS(x)^2 + LS(y)^2\}^{0.5}$.

Table 2
Metrical parameters for crystallographically characterized dimers in the CSD [29] involving [Pt{4′-(aryl)trpy}Cl]$^+$ cations, where the aryl group is a substituted or unsubstituted phenyl ring and the monomers are related by a crystallographic symmetry element (e.g., inversion).[a]

CSD Ref. code[b]	Type	MPS (Å)	Pt1···Pt2 (Å)	χ (°)	ψ (°)	LS(x) (Å)	LS(y) (Å)	%x displ.[c]	%y displ.[c]	LS(MPS) (Å)	LS (Å)	MMPD (Å)	Direction (°)[d]
FAZJOG_b	HH	3.325	3.301	94.4	81.4	−0.25	0.49	1.8	2.2		0.55	3.25	117.1
LABJOO_b	HH	3.366	3.352	91.1	84.5	−0.07	0.32	0.5	1.5		0.33	3.34	101.6
FAZJOG_a	HH	3.373	3.364	84.8	89.6	0.30	0.02	2.2	0.1		0.31	3.35	4.4
XIPNEP	HH	3.322	3.368	91.5	82.8	−0.09	0.42	0.6	1.9	0.55	0.43	3.34	101.6
VUYNEJ	HH	3.447	3.410	84.3	81.7	0.34	0.49	2.4	2.2		0.60	3.36	55.3
SAHHIT	HH	3.430	3.424	82.1	82.0	0.47	0.48	3.4	2.1		0.67	3.36	45.6
TW, Fig. 4b	HH	3.333	3.434	91.5	77.0	−0.09	0.77	0.6	3.5	0.83	0.78	3.35	96.5
LABJOO_a	HH	3.280	3.523	97.1	71.9	−0.44	1.09	3.1	4.9	1.29	1.18	3.32	111.8
XIPNIT	HH	3.408	3.573	83.2	73.7	0.42	1.00	3.0	4.5	1.07	1.09	3.40	67.0
LUNLIP_b	HH	3.317	3.608	94.4	69.9	−0.27	1.24	2.0	5.6	1.42	1.27	3.38	102.4
XIPNOZ_b	HH	3.453	3.629	87.9	72.6	0.13	1.08	0.9	4.9	1.12	1.09	3.46	83.1
FAZJUM_b	HH	3.390	3.661	81.6	66.7	0.54	1.45	3.9	6.5	1.38	1.55	3.32	69.7
XIPNOZ_a	HH	3.475	3.695	87.1	70.4	0.19	1.24	1.3	5.6	1.26	1.25	3.48	81.5
FAZJUM_a	HH	3.358	4.038	70.2	66.9	1.37	1.59	9.8	7.1	2.24	2.09	3.45	49.3
SIYPIA	HH	3.336	4.584	70.1	55.6	1.56	2.59	11.2	11.6	3.14	3.02	3.45	59.0
XULDOY	HH	3.511	4.611	59.7	67.2	2.33	1.79	16.7	8.0	2.99	2.94	3.55	37.5
LUNLIP_a	HT	3.258	7.130	32.4	75.5	6.02	1.79	43.1	8.0	6.34	6.28	3.38	16.5
TW, Fig. 4a	HT	3.241	7.632	38.0	66.3	6.02	3.07	43.1	13.8	6.91	6.76	3.55	27.0

[a] Abbreviations: HH, head-to-head; HT, head-to-tail; MPS, mean plane separation (measured as the distance between parallel 19-atom mean planes passing through the Pt atom and trpy ligand of each cation); χ, P2···Pt1—N1′ angle; ψ, P2···Pt1···C5 angle; LS(x) and LS(y) are the x- and y-components of the lateral shift (LS) vector, respectively, with the x-direction defined as the Pt—N1′ bond vector; LS(MPS), lateral shift calculated from the MPS and Pt1···Pt2 distance; LS, lateral shift calculated trigonometrically from LS(x) and LS(y); MMPD, metal-to-metal perpendicular displacement; TW, this work.
[b] Crystallographically unique dimers are distinguished by their CSD reference codes and a lower case label where two unique dimers exist.
[c] The % displacement reflects the magnitude of the x- and y-components of the LS vector relative to the x- and y-dimensions of a standard [Pt(trpy)Cl]$^+$ cation, namely 6.98 and 11.15 Å, respectively.
[d] The LS vector direction (angle) relative to the Pt–N1′ bond vector (i.e. the x-direction).

Table 3
Descriptive statistics for the 18 crystallographically characterized dimers listed in Table 2 involving [Pt{4′-(aryl)trpy}Cl]$^+$ cations, where the aryl group is a substituted or unsubstituted phenyl ring.[a]

	MPS (Å)	Pt1···Pt2 (Å)	χ (°)	ψ (°)	LS(x) (Å)	LS(y) (Å)	%x displ.	%y displ.	LS(MPS) (Å)	LS (Å)	MMPD (Å)	Direction (°)
Mean	3.368	4.074	79.0	74.2	1.03	1.16	8.3	5.2	2.35	1.79	3.39	68.2
SEM	0.018	0.298	4.4	2.0	0.46	0.19	3.2	0.8	0.57	0.45	0.02	8.0
SD	0.075	1.266	18.6	8.4	1.95	0.80	13.4	3.6	2.05	1.90	0.08	33.8
Variance	0.006	1.602	346.1	70.8	3.80	0.64	178.8	12.8	4.21	3.60	0.01	1141.1
Coefficient of Variance	0.022	0.311	0.2	0.1	1.90	0.69	1.6	0.7	0.87	1.06	0.02	0.5
Minimum	3.241	3.301	32.4	55.6	−0.44	0.02	0.5	0.1	0.55	0.31	3.25	4.4
Maximum	3.511	7.632	97.1	89.6	6.02	3.07	43.1	13.8	6.91	6.76	3.55	117.1
N	18	18	18	18	18	18	18	18	13	18	18	18

[a] For abbreviations and metrical parameter descriptors, refer to the footnote to Table 2 and Fig. 5.

tolyl)trpy}Cl]$^+$, we have analyzed the available data in the CSD [29] using the geometrical framework and parameters defined in Fig. 5. The results of this analysis are summarized in Tables 2 and 3. The Pt···Pt distances for 18 independent observations range from 3.30 to 7.63 Å; the mean metal-to-metal distance for this class of cations is towards the short end of the range at 4.1(1.3) Å (Table 3). The mean plane separation (MPS) averages 3.37(8) Å and is not highly variable (as evidenced by the small standard deviation, SD). The lateral shifts (LS) calculated trigonometrically from the Pt atom coordinates span a broad range (0.31–6.76 Å); the mean (1.79 Å) and SD (1.90 Å) reflect this, but do not portray the fact that cation pairs in this class of luminescent salts tend to cluster according to the type of dimer formed and consequently their characteristic LS (see below; Fig. 6).

It is noteworthy that a LS cannot be calculated from the Pt···Pt distance and MPS when the Pt···Pt interaction is very strong and the distance separating the metal ions is shorter than the MPS (e.g., when the trpy conformation is non-planar or, more specifically, concave with respect to the intradimer space) since this corresponds to a non-Pythagorean triangle. (Several dimers have no entry for the LS(MPS) value in Table 2 because of the foregoing condition.) In such cases, use of the x- and y-components of the LS vector to determine its direction and magnitude is mandatory and the plots in Fig. 6 have been made with LS values calculated in this manner. This method also allows calculation of the MMPD (metal-to-metal perpendicular displacement). It should be noted that the MMPD and MPS values can only be equivalent in the ideal case of perfectly planar [Pt(trpy)Cl]$^+$ cations making up a dimer. The MMPD values average 3.39(8) Å and are thus comparable in magnitude and range (though never identical) to the MPS values for this class of non-covalent dimers.

An important question to answer is whether or not the lateral shift for these dimers takes on a preferred orientation or direction relative to a particular molecular frame of reference. Calculation of the orientation of the LS vector relative to the x-axis is trigonometrically straightforward from the x- and y-components of the LS vector (Table 2). From Table 3, the LS vector exhibits a mean orientation of 68(34)° relative to the Pt–N1′ bond vector (x-direction). This suggests that, on average, the preferred displacement for this class of cations is 22° off the y-axis and over the first chelate ring within the trpy ligand (i.e. along a line connecting the Pt(II) ion to the midpoint of the N1–C2 bond of the first pyridine ring). The SD of the mean LS vector orientation is large because the cation···cation lateral shift direction is not confined to a particular region over the trpy ligand, but tends to cluster into three groups, from virtually over the x-axis to almost directly over the

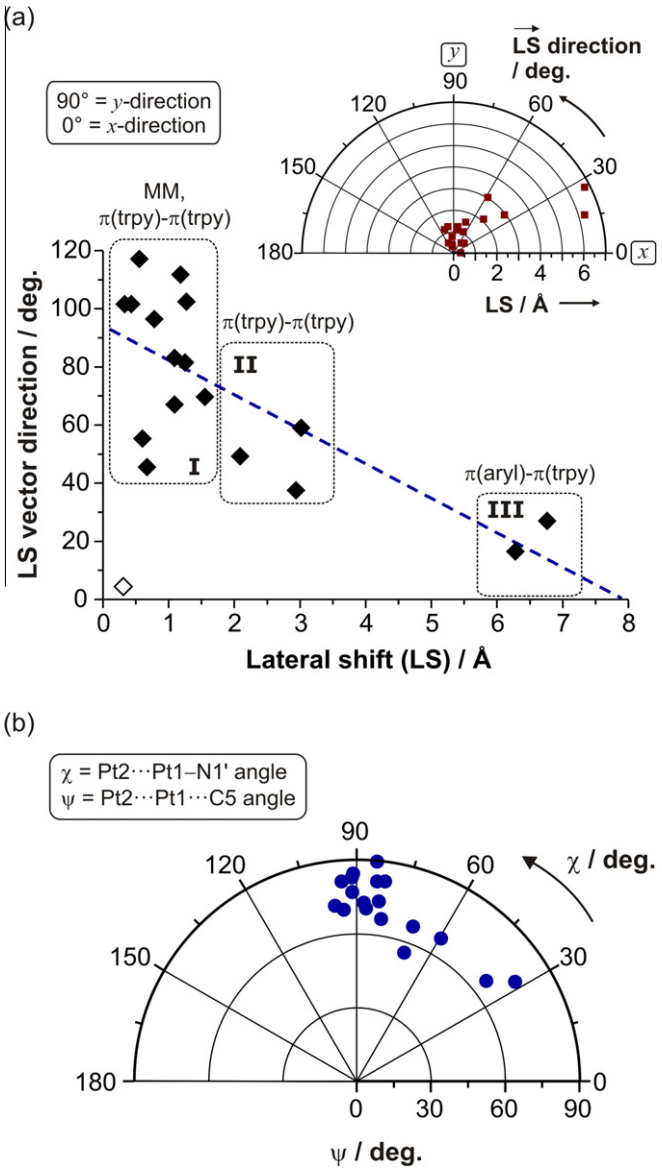

Fig. 6. (a) Plot of the lateral shift (LS) direction against the magnitude of the LS for the available crystallographically delineated $[Pt\{4'\text{-(aryl)trpy}\}Cl]^+$ cation dimers/stacks. Groups I–III reflect the dominant type of intermolecular interaction stabilizing the dimers. The dashed line illustrates the trend in the data as a linear least-squares fit, $f(x) = 94(7)–12(3)\ x$ (correlation coefficient = 0.74), without the outlying point (open diamond). The inset shows a polar plot of the same data over the full orientation range of the LS vector (0–180° due to the point group symmetry of the dimers). (b) Polar plot of the displacement angles χ and ψ (Fig. 5) for dimers comprising $[Pt\{4'\text{-(aryl)trpy}\}Cl]^+$ cations.

y-axis in the coordinate system used to quantify the dimer geometry. As discussed below, orientational clustering of the LS vector depends on the type of intermolecular interactions stabilizing $[Pt\{4'\text{-(aryl)trpy}\}Cl]^+$ cation pairs.

Fig. 6a shows both conventional and polar plots of the LS vector orientation against the magnitude of the LS. Despite the small size of the data set at present, several noteworthy points may be made from inspection of this plot: (i) the most common type of dimer formed by this class of cations is a *tight* head-to-head dimer with lateral shifts ranging from ~0.3 to ~1.55 Å and Pt···Pt distances ranging from 3.30 to 3.70 Å (Group I). The LS vectors for this class of dimers are mainly oriented between 45° and 120° (in the region encompassing the *y*-axis as depicted in Fig. 5, or roughly in the direction of the Pt–N1 bond). One salt (CSD code FAZJOG [9]) is an outlier in the sense that the LS is very short, but the LS vector displacement is along the *x*- rather than the *y*-axis (open diamond in Fig. 6a). As noted above and elsewhere [28], intermolecular interactions between cations falling into this group are dominated by a finite $d_z^2(Pt)$—$d_z^2(Pt)$ orbital interaction (MM) as well as π(trpy)–π(trpy) interactions. It is interesting to note that even with a lateral shift as large as 1.2–1.5 Å, this type of intermolecular interaction seemingly still holds presumably because the $5d_z^2$ orbitals are diffuse and a laterally offset head-on overlap (which, fundamentally, means that the interaction takes on more π-character) is not altogether unfavorable. (ii) A second group (Group II) of more loosely interacting head-to-head dimers is discernible from Fig. 6a (though with significantly fewer examples at present) and is characterized by LS values of 2–3 Å and LS vector orientations of between 30° and 60°. For these dimers, the LS is most likely too large to permit any significant side-on $d_z^2(Pt)$—$d_z^2(Pt)$ orbital interactions such that the key attractive forces between the platinum-bound trpy groups are π–σ electrostatic interactions [24,25], i.e. π(trpy)–π(trpy) overlap. (iii) A third group of cations (Group III) interact with the reverse geometry, namely head-to-tail, and in both examples form linear chains of cations stabilized by the overlap of the 4-aryl group with a flanking pyridine ring of the neighboring trpy ligand. For $[Pt\{4'\text{-}(p\text{-tolyl)trpy}\}Cl]SbF_6$, the distance between the centroids of the overlapping rings measures 3.594(2) Å. The long lateral shifts observed for the present salt and chloro-(2,2′:6′,2″-terpyridyl-4′-azobenzene)-platinum(II) hexafluorophosphate (CSD structure LUNLIP) [30], the only other example available at present in this group, are fully consistent with π(aryl)–π(trpy) interactions as the dominant stabilizing intermolecular interaction. The LS vector orientations for the present structure and LUNLIP are the most acute of all the complexes listed in Table 2, falling between 15° and 30°, and indicate that long lateral shifts preferentially occur along the *x*-axis direction of the chelate.

Although the data plotted in Fig. 6a are sparse in Groups II and III and quite scattered in Group I, the linear trend is not altogether unconvincing nor contrary to expectation. Indeed, the intercept is 90° within one standard deviation of the estimate and suggests that at very short lateral shifts for this class of dimers or stacks, the Pt(II) ion of one chelate is positioned slightly over the *y*-axis of the reference Pt(II) chelate with an appropriate MMPD. Interestingly, the straight line cuts the abscissa just short of a LS value of 8 Å. This suggests that dimers stabilized by π(aryl)–π(trpy) interactions have a LS displacement limit of about 8 Å and that this would be achieved when the Pt(II) ion of one chelate is positioned directly over the *x*-axis of the reference cation at an appropriate MPS. More specifically, such a geometry would involve overlap of the Pt(II) ion of one chelate with the 4′-(aryl) ring of the juxtaposed ligand and correspond to a finite and electrostatically favorable Pt(II)···π(aryl) interaction. Note that the distance from the Pt(II) ion to the centroid of the 4′-(aryl) ring of $[Pt\{4'\text{-}(p\text{-tolyl)trpy}\}Cl]SbF_6$ is 7.575(2) Å. A LS limit of around 8 Å (Fig. 6a) would position the Pt(II) ion of one chelate over the reference cation at an appropriate MPS and just beyond the centroid of the 4′-(aryl) ring along the line connecting this point to the *para*-C atom of the aryl ring. Although cation-π stabilizing interactions are well known for aromatic compounds and are indeed important in defining the tertiary and quaternary structures of proteins [31], an example of such a dimer with $[Pt\{4'\text{-(aryl)trpy}\}Cl]^+$ cations has yet to be observed. However, Pt(II)···π(aryl) interactions could be favoured for these chelates if non-bulky electron-donating groups occupied the *meta*-positions as well as the *para*-position on the 4′-aryl substituent of the trpy ligand—a situation that might permit substantial electrostatic attraction between the Pt(II) ion and the π-electron cloud of the 4′-(aryl) ring.

Finally, Fig. 6b shows a polar plot of the intradimer angles χ and ψ. The values of χ span the range 30–115° while the ψ-values are

confined to a narrower range of just over 30° from 56° to 90°. The broad range of χ-values is consistent with more facile cation slippage within a π–π dimer or π-stack along the *x*-axis direction (Pt–N1′ vector, Fig. 5). This phenomenon is also evident from the statistics in Table 3, which show that the χ-angle has the highest variance of all the direct parameters used to measure the interaction geometry. In real terms, however, 72% of the complexes analyzed fall into Group I and have χ-values spread over a much narrower, more orthogonal range of 81–90°. The Group II and III cation dimers without Pt···Pt interactions are in the minority, but are clearly responsible for the high variance of χ. One other noteworthy observation is that only 33% of the cation pairs exhibit obtuse values of χ. In other words, slippage in a negative *x*-direction (along the Pt–Cl bond vector) is generally less common than a lateral shift in the opposite direction.

3.3. Solid state photophysics of [Pt{4′-(*p*-tolyl)trpy}Cl]SbF$_6$

The absorption and emission spectra of the [Pt{4′-(*p*-tolyl)trpy}Cl]$^+$ cation have been previously recorded in acetonitrile [1]. We report in Section 2 the absorption and emission spectra of the cation measured in dichloromethane. Dichloromethane was chosen because it is a non-coordinating solvent with a lower dielectric constant than acetonitrile and, on this basis, should afford an emission spectrum that more closely resembles one measured for the cation in the solid state. The spectrum fits the profile for emission from a ^{3}MLCT state, the same assignment made by Yip and co-workers [1]. The emission maximum (for the 0–0 transition) occurs at 545 nm and there is a shoulder at 580 nm, easily assigned to the 0–1 transition. These data help in the interpretation of the emission spectrum recorded on an analytically pure micro-crystalline powder sample of [Pt{4′-(*p*-tolyl)trpy}Cl]SbF$_6$ (Fig. 7). Note that it was necessary to record the spectrum at 77 K in order to obtain a sufficiently intense signal; in fact, even at 77 K, some difficulty was experienced in obtaining a satisfactory signal to background ratio.

The spectrum shown in Fig. 7 displays three main features. There is a relatively sharp and intense peak at 550 nm, a broader and somewhat more intense peak at 610 nm; and a third that exhibits as a pronounced shoulder at ~650 nm. We have measured excited state lifetimes for the emissions at 550, 610 and 650 nm. For the first two peaks the intensity decay curve was biphasic, affording lifetimes of 1.46(1) and 7.59(7) μs for the 550 nm emission; and 3.87(4) and 11.4(3) μs for the 610 nm emission. For the 650 nm emission a good fit with a single-exponential decay curve was obtained, affording a lifetime of 4.832(5) μs. The complexity of the emission spectrum, as well as the biphasic nature of the intensity decay curve for the first two peaks, clearly indicate that emission from more than one excited state is being recorded in the solid state. To try and identify these separate excited states we have deconvoluted the spectrum in Fig. 7 into its Gaussian components. This is also shown in Fig. 7, along with the experimental and calculated spectra. The first Gaussian component (colored blue) maximizes at 554 nm, a close fit with the emission maximum of 545 nm measured for the complex in dichloromethane solution. On this basis we assign the 550 nm peak to emission from a ^{3}MLCT excited state that has its origins in monomer excitation. The second Gaussian peak (colored green) maximizes at 604 nm, and is relatively narrow with a full-width-at-half maximum value of 1373(55) cm^{-1}; it is red-shifted by ~60 nm from the ^{3}MLCT peak, both indications that the peak has its origins in a dσ*–π* excitation, i.e. this emission is from a ^{3}MMLCT (metal–metal-to-ligand charge transfer) excited state [1,5,6,8,9,11,27,32–35]. Consistent with this assignment is the observation in the crystal structure of a Pt···Pt distance that is short enough (3.434(1) Å, Fig. 4) to support a stabilizing d_z^2(Pt)—d_z^2(Pt) orbital interaction. In fact, this band is, both in terms of energy and profile, typical of the kind of solid emission exhibited by planar complexes of platinum(II) that have crystal structures containing Pt_2 dimers: see [Pt(trpy)Cl]CF_3SO_3 (λ_{em}^{max} = 625 nm at 77 K) [1] and [(2,6-di-(2′-naphthyl)-4-pyridine)Pt_2{μ-bis(diphenylphosphino)methane}] (λ_{em}^{max} = 602 nm) and its solvates [36]. Two further Gaussian bands are necessary to fit the experimental spectrum. One (solid red line) is broad, and maximizes at 645 nm, while the other (broken red line) is even broader, relatively weak and maximizes at the longer wavelength of 673 nm. Assignment of these two peaks is less straightforward. However, we suspect that they both derive from a single emitting state, in view of the single lifetime measured for the 650 nm peak, and that the "extra" peak at 673 nm is simply a vibrational component. We speculate that this emission derives from an excimeric ^{3}π–π* excited state. Consistent with this assignment is the broadness and relatively low energy of the emission, and that there are, indeed, π(aryl)–π(trpy) interactions in the crystal (*vide supra*). Similar excimeric emission has been recorded in the solid state for other complexes of platinum(II) with aromatic ligands [4,5,28a,37]. Furthermore, from close inspection of the Pt···Pt interactions in the solid-state structure of [Pt{4′-(*p*-tolyl)trpy}Cl]SbF$_6$ (Fig. S1, Supporting Information), we find that there are no additional Pt···Pt interactions shorter than 3.434(1) Å that could yield a second, lower-energy ^{3}MMLCT state ⩾ 650 nm in the emission spectrum of the solid.

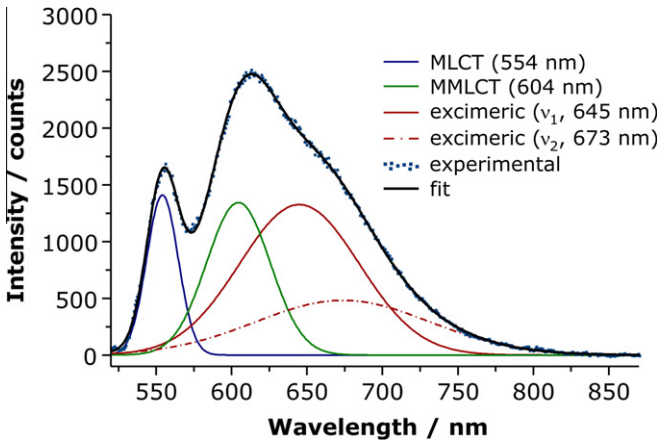

Fig. 7. Emission spectrum recorded on a microcrystalline sample of [Pt{4′-(*p*-tolyl)trpy}Cl]SbF$_6$ at 77 K: λ_{ex} = 420 nm. The emission envelope has been corrected for background glass emission. Also shown are the Gaussian bands obtained by deconvolution of the spectrum, and the spectrum calculated using these bands (r^2 = 0.9994, fit std. error 21.8).

4. Concluding remarks

This work illustrates the idea that the photo-excited state properties of a material are dependent on the environment of the chromophore in the solid state, i.e. on the crystal structure of the material and, more specifically, on the nature of the intermolecular interactions that link the chromophores (arrays of [Pt{4′-(*p*-tolyl)trpy}Cl]$^+$ cation pairs or dimers in the present case). Interestingly, X-ray photocrystallographic analysis is now used to quantify the relationship between environment and the nature of the emitting state, the best characterized examples being of gold(I) phosphine complexes [38]. These studies show directly the effect of crystal structure on the structural changes that occur on photo-excitation of the material, and hence on the emission properties of the material [38]. As far as luminescent platinum terpyridine complexes are concerned, there has not been the same detailed inves-

tigation, though there are examples in the literature for which there is a clear relationship between crystal structure and photophysical properties, usually between the strength of a stabilizing Pt···Pt interaction (measured by the Pt···Pt distance) and the emission wavelength of the material [5,6,8–10]. However, as this work further exemplifies, multiple emissions are not uncommon in materials of this type [7,8,39]—a complicating factor in any systematic investigation and certainly a limitation on their potential use as optical devices.

Acknowledgements

The authors thank the South African National Research Foundation and the University of KwaZulu-Natal for financial support. Our thanks also go to Judith Magee of the Department of Chemistry, Durham University, UK for the elemental analyses.

Appendix A. Supplementary material

CCDC 802514 contains the supplementary crystallographic data for [Pt{4′-(p-tolyl)trpy}Cl]SbF_6. These data can be obtained free of charge from The Cambridge Crystallographic Data Centre via www.ccdc.cam.ac.uk/data_request/cif. Fig. S1 (close-up view of cation-to-cation interactions within a staircase packing motif) and Fig. S2 (metrical parameters for a linear chain of laterally-shifted dimers). Supplementary data associated with this article can be found, in the online version, at doi:10.1016/j.ica.2011.03.043.

References

[1] H.-K. Yip, L.-K. Cheng, K.-K. Cheung, C.-M. Che, J. Chem. Soc., Dalton Trans. (1993) 2933.
[2] D. Zhang, L.-Z. Wu, L. Zhou, X. Han, Q.-Z. Yang, L.P. Zhang, C.H. Tung, J. Am. Chem. Soc. 126 (2004) 3440.
[3] P. Du, J. Schneider, F. Li, W. Zhao, U. Patel, F.N. Castellano, R. Eisenberg, J. Am. Chem. Soc. 130 (2008) 5056.
[4] J.A. Bailey, M.G. Hill, R.E. Marsh, V.M. Miskowski, W.P. Schaefer, H.B. Gray, Inorg. Chem. 34 (1995) 4591.
[5] J.S. Field, R.J. Haines, D.R. McMillin, G.C. Summerton, J. Chem. Soc., Dalton Trans. (2002) 1369.
[6] J.S. Field, J.-A. Gertenbach, R.J. Haines, L.P. Ledwaba, N.T. Mashapa, D.R. McMillin, O.Q. Munro, G.C. Summerton, J. Chem. Soc., Dalton Trans. (2003) 1176.
[7] R. Büchner, J.S. Field, R.J. Haines, L.P. Ledwaba, R. McGuire Jr., D.R. McMillin, O.Q. Munro, Inorg. Chim. Acta 360 (2007) 1633.
[8] J.S. Field, L.P. Ledwaba, O.Q. Munro, D.R. McMillin, CrystEngComm 10 (2008) 740.
[9] T.J. Wadas, Q.-M. Wang, Y.-J. Kim, C. Flaschenreim, T.N. Blanton, R. Eisenberg, J. Am. Chem. Soc. 126 (2004) 16841.
[10] P. Du, J. Schneider, W.W. Brennessel, R. Eisenberg, Inorg. Chem. 47 (2008) 69.
[11] R. PyBüchner, C.T. Cunningham, J.S. Field, R.J. Haines, D.R. McMillin, J. Chem. Soc., Dalton Trans. (1999) 711.
[12] K.M.-C. Wong, N. Zhu, V.W.-W. Yam, Chem. Commun. (2006) 3441.
[13] V.W.-W. Yam, K.M.-C. Wong, N. Zhu, J. Am. Chem. Soc. 124 (2002) 6506.
[14] F. Kröhnke, Synthesis (1976) 1.
[15] Felix32© Analysis Version 1.1 (build 51 Beta 8), Program for the Analysis of Emission Spectra, Photon Technologies International, Birmingham, NJ 08011, USA, 2003.
[16] Oxford Diffraction Ltd., Abingdon, Oxford OX14 1RL, UK, 2003.
[17] G.M. Sheldrick, Acta Crystallogr., Sect. A64 (2008) 112.
[18] L.J. Farrugia, J. Appl. Crystallogr. 30 (1997) 565.
[19] ORTEP3 for Windows: L.J. Farrugia, Department of Chemistry, University of Glasgow, Glasgow, G12 8QQ, UK, 2001.
[20] I.J. Bruno, J.C. Cole, P.R. Edington, M. Kessler, C.F. Macrae, P. McCabe, J. Pearson, R. Taylor, Acta Crystallogr., Sect. B58 (2002) 389.
[21] K.W. Jennette, T.J. Gill, J.A. Sadownick, S.J. Lippard, J. Am. Chem. Soc. 98 (1976) 6159.
[22] V.W.-W. Yam, R.P.-L. Tang, K.M.-C. Wong, K.-K. Cheung, Organometallics 20 (2001) 4476.
[23] H. Jude, J.A.K. Bauer, W.B. Connick, J. Am. Chem. Soc. 125 (2003) 3446.
[24] C.A. Hunter, J.K.M. Sanders, J. Am. Chem. Soc. 112 (1990) 5525.
[25] C. Janiak, J. Chem. Soc., Dalton Trans. (2000) 3885.
[26] J.S. Field, C.D. Grimmer, O.Q. Munro, B.P. Waldron, Dalton Trans. 39 (2010) 1558.
[27] W.B. Connick, R.E. Marsh, P. Schaefer, H.B. Gray, Inorg. Chem. 36 (1997) 913.
[28] (a) D.S. Martin, Extended interactions between metal ions, in: L.V. Interannte (Ed.), ACS Symp. Ser. 5, American Chemical Society, Washington, DC, 1974, p. 254.;
(b) V.M. Miskowski, V.H. Houlding, Inorg. Chem. 28 (1989) 1529.
[29] F.H. Allen, Acta Crystallogr., Sect. B58 (2002) 380.
[30] T. Yutaka, I. Mori, M. Kurihara, J. Mizutani, N. Tamai, T. Kawai, M. Irie, H. Nishihara, Inorg. Chem. 41 (2002) 7143.
[31] S. Mecozzi, A.P. West Jr., D.A. Dougherty, Proc. Natl. Acad. Sci. USA 93 (1996) 10566.
[32] J.S. Field, R.J. Haines, D.R. McMillin, O.Q. Munro, G.C. Summerton, Inorg. Chim. Acta 358 (2005) 4567.
[33] W.B. Connick, L.M. Henling, R.E. Marsh, H.B. Gray, Inorg. Chem. 35 (1996) 6261.
[34] S.-W. Lai, M.C.-W. Chang, T.-C. Cheung, S.-M. Peng, C.-M. Che, Inorg. Chem. 38 (1999) 4046.
[35] M. Kato, C. Kosuge, K. Morii, J.S. Ahn, H. Kitagawa, T. Mitani, M. Matsushita, T. Kato, S.S. Zillian, H.G. Yano, M. Kimura, Inorg. Chem. 38 (1999) 1638.
[36] S.C.F. Kui, S.S.-Y. Chui, C.-M. Che, N. Zhu, J. Am. Chem. Soc. 128 (2006) 8297.
[37] (a) K.-T. Yam, C.-M. Che, K.-C. Cho, J. Chem. Soc., Dalton Trans. (1991) 1077;
(b) H. Kunkely, A. Vogler, J. Am. Chem. Soc. 112 (1990) 5625.
[38] (a) M. Hoshino, H. Uekusa, S. Sonada, T. Otsuka, T. Kaizu, Dalton Trans. (2009) 3085;
(b) M. Hoshino, H. Uekusa, Y. Obashi, Bull. Chem. Soc. Jpn. 79 (2006) 1362;
(c) M. Hoshino, H. Uekusa, S. Ishii, T. Otsuka, Y. Kaizu, Y. Ozawa, K. Toriumi, Inorg. Chem. 49 (2010) 7257.
[39] R. Büchner, J.S. Field, R.J. Haines, C.T. Cuninngham, D.R. McMillin, Inorg. Chem. 36 (1997) 3952.